International Journal on Advanced Science Engineering Information Technology

Vol.8 (2018) No. 5
ISSN: 2088-5334

Classification of Alzheimer's Disease in PET Scans using MFCC and SVM

Jantana Panyavaraporn[#], Paramate Horkaew[*]

[#]*Department of Electrical Engineering, Burapha University, 169 Saensook, Mueang, Chon Buri, 20131, Thailand*
E-mail: jantana.p@eng.buu.ac.th

**School of Computer Engineering, Suranaree University of Technology, 111 University Avenue Muang, Nakorn Ratchasima, 30000, Thailand*
E-mail: phorkaew@sut.ac.th

***Abstract*—Unlike age-related dementia, Alzheimer's disease is more progressive and causes rapid deterioration in a patient's cognitive functions. Before its first clinical manifestation, it is evident that the damaging brain process has already been commenced much earlier in life. This asymptomatic period could have spanned as long as a decade or more. Although there is not yet an ultimate cure for the disease, the sooner it is diagnosed, the more chance that available therapeutic measures could improve the patient's quality of life. Standard medical questionnaire and medical imaging are the principal means of identifying early Alzheimer's disease. Despite a great effort having been made in analyzing structural atrophy in the human brain by using CT and MRI, the recent attempts have reached high accuracy and precision but relatively poor sensitivity. Functional imaging such as PET is of much lower spatial resolution but promising modality taken to elevate this limitation. This paper presents a classification method for early detection of the disease from PET scans drawn from the Thai population. However, instead of conventional structural analysis, this study performed clustering on unwrapped signals, transformed from imaging data by using Mel-Frequency Cepstral Coefficients (MFCC), by a generic Support Vector Machine (SVM) classifier. The experimental results reported herein indicate that, with the optimal MFCC order, the proposed method could identify subjects with Alzheimer's from controls, with high accuracy, precision, and specificity. With a cross-validation ratio of 8:2 and a linear SVM kernel, the classification accuracy, sensitivity, and specificity were 96.51, 93.98, and 97.77, respectively, and increased as the MFCC orders.**

***Keywords*—PET images; Alzheimer disease; MFCC; SVM.**

I. INTRODUCTION

Rapid transition into a fully developed aging society has currently been undergoing, and its sign has become ever more apparent in the last few years when a drastic drop in the ratio between children and mature adults' population has constantly been reported. Among common measures taken in response to such an event, healthcare services for older adults have to be readily prepared. The most common diseases from which older adults are suffered include high blood pressure, high cholesterol, and dementia. More particularly the latter, there are 47 million people to date live with dementia worldwide. It is projected that by 2050, the number is to increase to more than 131 million, as population been aging [1]. Dementia is diagnosed by the loss of cognitive functioning such as thinking, remembering, and reasoning, and behavioral abilities to such an extent that it interferes with the patient's daily life. Depending on the types of neurological degradation [2], Dementia can be categorized by its causes. Unlike age-related dementia that is gradually developed as aging progresses, Alzheimer's disease (AD) is much more severe and considered the most common cause, i.e., about 60 to 80 percentages of diagnosed cases [3].

Alzheimer disease is a progressive brain disorder that damages memory and thinking functions, and eventually the ability to carry out even the most straightforward task. In most people with Alzheimer's, related symptoms only first appear in their mid-60s, when their memory and other cognitive malfunctions are noticeable. It is however likely that damages had already been caused in their brain even much earlier, probably a decade or more. During this preclinical AD stage, patients seem healthy, but toxic changes have already started. They include abnormal deposits of proteins form amyloid plaques and tau tangles throughout the patient's brain, and once-healthy neurons stop functioning, lose connections with other neurons, and die [4]. During clinical interview, patients in the early-stage AD are associated with struggling to remember recent conversations, names or events. Apathy and depression are

also symptoms commonly manifest. As the disease progresses, patients begin to experience impaired communication, disorientation, poor judgment, confusion, changes in behavior. Eventually, they will be suffered from difficulty in even simple tasks, such as speaking, swallowing and walking [3]. It is widely accepted that early diagnosing of the AD enables effective therapeutic measures that can improve patient's quality of life.

In addition to the clinical survey, medical imaging is typically adopted in early diagnosing of the AD. Visual and computerized techniques found in literature adopted Magnetic Resonance Imaging (MRI), Computed Tomography (CT), Positron and Single Positron Emission Tomography (PET and SPECT). Imaging brain structural changes by using MRI and enhanced CT yielded relatively high accuracy and precision. The most prevailing technique is the shape analysis of the hippocampus to characterize its atrophy. Threshold value could be imposed on hippocampus area to differentiate symptomatic instances from controls. Thanks to their high spatial resolution MRI and CT offer excellent detection accuracy and precision. However, without more articulate morphological metrics [5], these modalities suffer from low sensitivity, and hence unsuitable for early AD detection. Functional imaging, such as PET and SPECT, uses the radioactive material as a biological tracer in cells [6]. It enables a physician to visualize AD-related chemical changes occur in the brain. An extensive review of the diagnostic value of FDG and amyloid PET in Alzheimer's disease can be found in the recent article by Rice et al. [7]. Specifically, AD diagnostic criteria include the neuron degeneration markers measurable by FDG-PET and those of amyloid accumulation measurable by amyloid-PET. It was shown in the study that both techniques were able to detect AD with high sensitivity and specificity when validated with other neurodegenerative processes and normal age-related cognitive disorders.

Computerized image analysis of PET scans (and also those fused with MRI) for early diagnosis of Alzheimer's disease was reported in the literature [8]–[13]. The main characteristics regarding feature extraction, classification, and image database are summarized and compared in Table I. In [8], [9], the novel classification methods were focused. Lu et al. [8] proposed a novel multiscale deep neural network (MDNN) to learn the patterns of metabolism changes due to AD pathology in FDG-PET images and use them as the discriminant between AD subjects and normal controls (NC). Based on the data published by Alzheimer Disease Neuroimaging Initiative (ADNI) the deep architecture performed well, especially in early AD cases. Wu et al. [9] improved the AD prediction accuracy by combining 3 different classifiers, i.e., K-Nearest Neighbors (KNN), Random Forests, Neural Network, by using weighted and unweighted schemes. They reported that the weighted ensemble models outperformed individual models with overall cross-validation accuracy of 86.1%.

In [10], Cheng and Liu proposed a novel classification framework based on a combination of 2D convolutional neural networks (CNN) and recurrent neural networks (RNN). In this work, the 2D CNN was built to capture intra-slice features, while the gated recurrent unit (GRU) of RNN was used to extract inter-slice features for final classification. This method was evaluated on the baseline PET images, and the results showed that it was able to achieve a high classification accuracy of up to 95%.

In addition to the classification method, feature extraction also played an equally crucial part in AD diagnosis. Elman Back Propagation Neural Network (EBPNN) was proposed in [11] for AD classification. In that study, PET and MRI data were also obtained from ADNI. The PET and MRI images were preprocessed by Wiener filter and had their features extracted by using a trivial Gray-Level Co-occurrence Matrix (GLCM). Similarly, another work [12] ranked the effectiveness of multiple brain regions to separate AD from healthy controls. With this method, a brain image was first mapped into 116 anatomical regions of interest (ROI). The first four moments and the entropy of histograms of these regions were then computed. Receiver Operating Characteristics (RoC) curves were later employed to rank the regional effectiveness (or ability) to separate the images. Out of 116, 21 regions were selected as input to both Support Vector Machine (SVM) and Random Forest classifiers. In [13], features within ROI were extracted by using scale-invariant Laplacian of Gaussian (LoG) operator and then classified by using SVM and its probabilistic variant (pSVM). In both studies, PET images were also obtained from the ADNI database.

TABLE I
SUMMARY OF CLOSELY RELATED COMPUTER-AIDED DIAGNOSES OF ALZHEIMER'S DISEASE FROM PET SCANS

#Ref.	Feature Extraction	Classification	Databases
[8]	-	MDNN	PET/ ADNI
[9]	-	KNN, Random Forests, Neural Networks	PET/ ADNI
[10]	Intra- and inter-slice features	2D-CNN and RNN	PET/ ADNI
[11]	GLCM	EBPNN	PET and MRI/ ADNI
[12]	Local moments and entropy of histograms	SVM and Random Forest	PET/ ADNI
[13]	LoG	SVM and pSVM	PET/ ADNI

Support Vector Machine (SVM) is a supervised machine learning (ML) algorithm. There have been studies that applied SVM for classification problems [14]-[16]. Byun [14] presented a survey on applications of SVM for pattern recognition. To name a few, SVM was applied to solar irradiance prediction [15] and cancer diagnosis [16].

It is worth stressing here that the success of computer-aided diagnosis in the early AD is highly dependent on preprocessing, including segmentation and feature extraction. This paper thus proposes a novel feature extraction by Mel-Frequency Cepstral Coefficients (MFCC). The technique has been highly reputed for being able to emulate human perception by non-linearly decompressing spectral bands. This, in turn, allows for a better representation of the underlying signals. Since signal spectra were equally spaced in Mel scale, they can be composed and effectively used as a feature vector for subsequent analyses. MFCC has been successfully applied in both audio and speech recognition applications [17].

This paper is organized as follows. Section II discusses the characteristic of PET imaging data and detailed description of the proposed method. The experimental

results are reported and discussed in Section III. Finally, the relevant concluding remark is made in Section IV.

II. Material and Method

This paper focuses on feature extraction and classification of imaging signal for early AD diagnosis from PET scans. The imaging data employed in this study was acquired from Thai participants who were diagnosed of the AD condition and the normal controls, with informed consent. The proposed scheme consists of (1) brain ROI segmentation by K-mean clustering, (2) 2D image to 1D signal unwrapping, (3) Mel-Frequency Cepstral Coefficients (MFCC) based feature extraction, and (4) Support Vector Machine (SVM) for AD classification. The process is outlined in Fig. 1 and detailed descriptions are given in the following subsections.

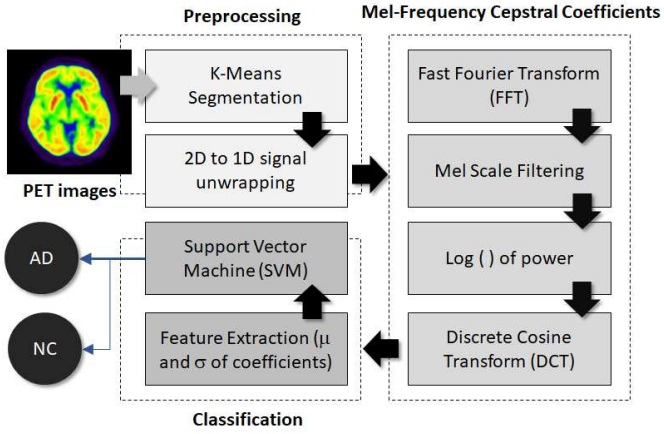

Fig. 1 Diagram outlining the proposed scheme

A. Data Preparation

The brain images employed in the following experiment were obtained from a local university hospital. They were multi-slice PET brain scans of 30 subjects, stored in DICOM format. The pixel depth of each image was 16 bits per pixels. These PET images were grouped into 2 classes, namely (a) standard controls (NC) and (b) Those diagnosed with the AD (AD), consisting of 20 and 10 subjects, respectively. Single slice per subject was chosen to cover related peripherals by a medical expert. Examples of NC and AD slices are shown in Fig. 2.

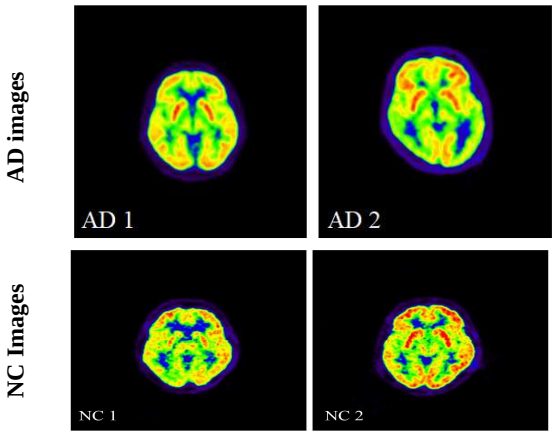

Fig. 2 Examples of the AD (top) and NC (bottom) PET scans

B. Brain Segmentation

To focus on imaging signal only within ROI, background needed to be cropped out. Any trivial segmentation methods could be employed for this task. Without loss of generality, a simple K-means clustering opted in this study. More specifically, two points were randomly placed on an image as the initial centroids, i.e., pixel intensities at the corresponding loci. For each pixel in the image, find the nearest centroid and then update its value to the center of the cluster, taking into account the newly added pixel. The process was repeated until the centroids reached their convergence, as depicted in Fig 3.

The expression of K-means calculation is given below:

$$s = \sum_{j=1}^{k}\sum_{i=1}^{n}\left\| x_i^{(j)} - c_j \right\|^2 \quad (1)$$

Where k is the number of clusters, n is the number of pixels, x is input data and c are centroids.

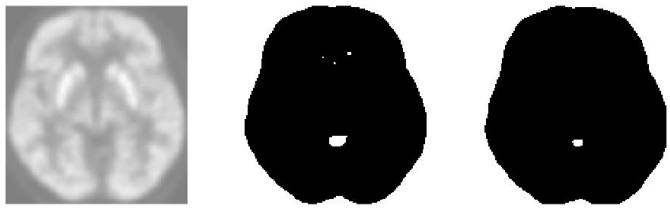

Fig. 3 Example of K-means brain segmentation showing (a) cropped brain and its binary image after 2 (b) and 15 (c) iterations upon convergence

C. Feature Extraction

From Fig. 2, the AD is manifest as a distinct pattern of activity than NC, which could be assessed by respective local texture properties. Unlike some existing PET studies, where spatial descriptors were used to characterize the underlying texture explicitly, this study took a spectrum analysis approach instead. In the frequency domain, the spectrum of PET activity map was locally compressed, and AD-NC differences were evident when visually observed, but somewhat indistinctive in linear scale. MFCC was, therefore, a viable choice for texture spectrum decompressor. The MFCC [17] is a feature extraction method first proposed in the 1980s and widely applied in speech recognition applications. With MFCC, frequency spectra of a truncated signal were first extracted and spaced by Mel filter banks into several bands, which got more extensive as the frequencies increased. Accordingly, low spectra with higher energy had a more considerable degree of separation than higher ones. The resultant energy at each band was then transformed into a logarithmic scale, to match the human sensory system and to allow Cepstral mean subtraction during feature normalization. DCT was finally applied to decorrelate filter bank energies, so that respective covariance matrix could be used to model the features in subsequent analyses. Since PET image was a 2D signal, it was first unwrapped into the 1D signal. The detailed expressions of the MFCC steps were provided as follows:

1) The spectrum of an unwrapped signal was computed by using the Fast Fourier Transform (FFT) as per Eq. 2.

$$x(k) = \sum_{n=0}^{N-1} x(n) \cdot W_N^{kn} \quad (2)$$

where $W_N^{kn} = e^{-\frac{j2\pi}{N}}; k = 0,1,...,N-1$ and $x(n)$ is a 1D signal and $x(k)$ is output signal.

2) The resultant power spectra were non-linearly spaced by Mel filter banks and mapped onto a logarithmic scale.
3) The energies spectra were decorrelated by using Discrete Cosine Transform (DCT) as per Eq. 3.

$$y(k) = \sqrt{\frac{2}{N}} \sum_{n=0}^{N} x(n) \cdot \frac{1}{\sqrt{1+\delta_{k1}}} \cdot \cos\left(\frac{\pi}{2N}(2n-1)(k-1)\right) \quad (3)$$

where $x(n)$ is the input signal, N is its length, $y(n)$ is the output signal and δ_{k1} is the Kronecker delta.

4) The amplitudes of the resultant spectral, called cepstral coefficients were used for the subsequent classification.

D. Classification

Depending on the width of an ROI extracted and traversed into the 1D signal as described in sections B and C, the number of Cepstral coefficients per each subject varies. Fig. 4 depicts the Cepstral coefficient vectors of one subject, selected from NC (a) and AD (b) datasets. Fig. 4(a) and 4(b) consist of 108 and 149 coefficient vectors, respectively. Visual inspection reveals notable discriminate patterns between both groups.

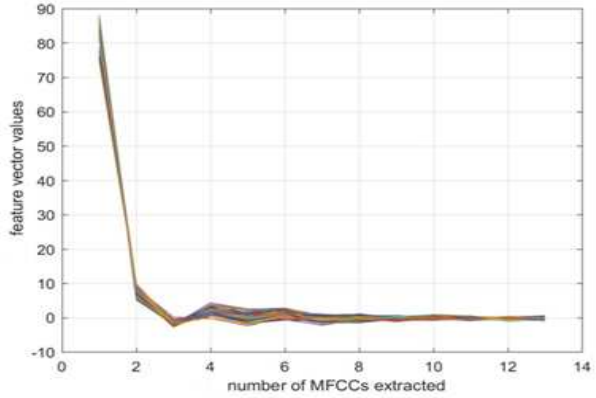

(a) Normal Control (NC) subject

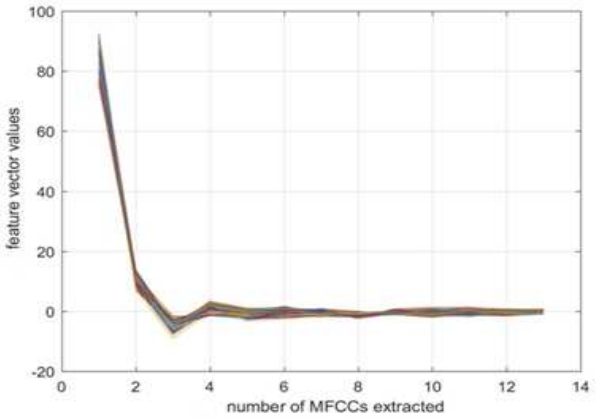

(b) Alzheimer's Disease (AD) subject

Fig. 4 The first 13 orders of extracted cepstral coefficients of (a) NC subject consisting of 108 vectors and (b) AD subject consisting of 149 vectors.

However, because discrepancies at higher orders tended to diminish (i.e., the difference between consecutive orders was less than 0.2% on average), only the first 13 orders were thus used and shown here. Since the signal length extracted from different subjects varied as the ROI, the size of the coefficient vector also varied. It is evident from figure 4(a) and 4(b) that, despite such difference, the coefficients in each subject are clustered and followed the similar trend. In order to eliminate variations in the numbers of coefficients, their mean and standard deviation vectors were calculated as per Eq. 4 and 5 and used as a feature vector in the SVM classification.

$$\bar{x} = \frac{\sum_{i=1}^{N} x_i}{N} \quad (4)$$

$$SD = \sqrt{\frac{\sum_{i=1}^{N} (x_i - \bar{x})^2}{N-1}} \quad (5)$$

Where $x_1, x_2, ..., x_N$ are cepstral coefficients, $\bar{x}$ is mean, SD is a standard deviation and N is the number of Cepstral coefficients extracted from a given subject.

Support Vector Machine (SVM) is a supervised machine learning algorithm which can be used for classification. In the proposed scheme SVM was employed to classify AD versus NC images based on obtained feature vectors, i.e., means and standard deviations of extracted Cepstral coefficients.

III. Results and Discussion

This section provided a detailed account of the performance evaluation and experimental setups. Relevant numerical and graphical results are given and discussed. For benchmarking, the classification results obtained from the proposed method was compared against those from a CNN classifier.

A. Performance Evaluations

To evaluate the proposed scheme, classification accuracy (A_c) for an image being a member of a given class, containing N a sample, was defined as

$$A_c = n/N \quad (6)$$

where n is the number of correctly classified samples and N is the total number of samples in that class.

A total of 30 subjects were recruited and analyzed in this study. They were divided into 2 classes, i.e., those diagnosed with Alzheimer's disease (AD) and the healthy normal controls (NC), consisting of 10 and 20 subjects (images), respectively. In the following experiments, cross-validation was employed. Cross-validation aimed to confirm that the revised model was not overfitted and thus could generalize to allow an unseen instance, despite the limited size of the training set. Leave-p-out cross-validation involves using p observations as the validation set and those remaining as the training set. This process was repeated by training the classification model from the original dataset, but with p samples removed in turn. The total number of exhaustive training and validation iterations is given by C_p^n, as expressed in Eq. 7.

$$C_p^n = \frac{p!}{(n-p)!p!} \quad (7)$$

Where n is the number of observations in original sample.

B. Experimental Setup

The experiments reported herein were based on the model implemented on MATLAB. Due to limit number of available PET scans, SVM was therefore preferred as it is known for being reliable against overfitting. Nonetheless, to objectively confirm this statement, the Leave-p-out mentioned above cross-validation was carried out. In the first experiment, the ratio between training and testing images were set to 70:30, 80:20, and 90:10, respectively. For example, in the 80:20 case, 80 percentages of NC and AD were drawn from respective classes and used as the training set. That is 8 out of 10 AD and 16 out of 20 NC subjects were included in this set. Accordingly, the number of model validation was given by $C_8^{10} \times C_{16}^{20}$ or 218,025 iterations. Similarly, in the 90:10 case, the total number of iterations equaled $C_9^{10} \times C_{18}^{20}$ or 1,900. The model performance for SD and mean features were then evaluated, per each ratio, based on standard metrics, i.e., accuracy (Acc.), sensitivity (Sens.) and specificity (Spec.). The results are listed in Table II and III.

TABLE II
ACCURACY, SENSITIVITY, AND SPECIFICITY OBTAINED FROM THE PROPOSED METHOD BY USING A LINEAR KERNEL SVM

	Number of Experiments	Ratio (%)	Acc. (%)	Sens. (%)	Spec. (%)
SD	4,651,200	70:30	95.33	92.77	96.62
	218,025	80:20	96.51	93.98	97.77
	1,900	90:10	98:07	96.11	99.05
Mean	218,025	80:20	100	99.99	100
	1,900	90:10	100	100	100

C. Discussions

The number of cepstral coefficients was determined by the width of brain ROI which varied across subjects. Thus, in order to normalize the feature vector, its mean and standard deviation at respective orders were computed for each subject. Fig. 5 illustrates the comparison between AD and NC subjects based on the first 5 MFCC orders of Mean (Fig. 5(a)) and Standard Deviation (Fig. 5(b)) feature vectors. Each bar represents a variation (min-max) across dataset per each order.

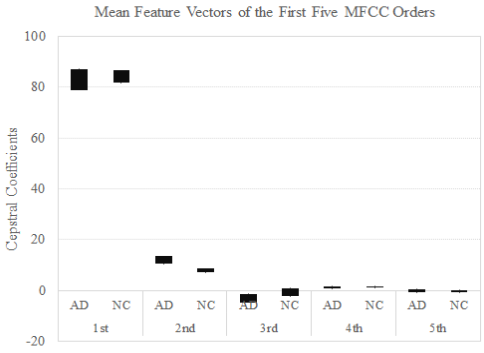

(a) Mean Feature Vectors

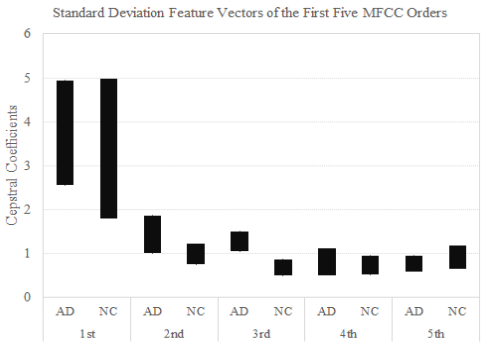

(b) Standard Deviation Feature Vectors

Fig. 5 Comparison of between AD and NC based on Mean (a) and Standard Deviation (b) feature vectors. For clarity, only the first five orders are shown.

It is clear that there exist discrimination patterns between AD and NC groups on both feature vector spaces. In order to elucidate this observation, the respective 3D scatter plots of each feature vector are depicted in Fig. 6. The class separations are evident in both plots., another experiment similar to Section B. was carried out for 80:20 validation but with different types of kernels to determine suitable kernel used in SVM.

TABLE III
ACCURACY, SENSITIVITY, AND SPECIFICITY OBTAINED FROM SVM CLASSIFICATION WITH DIFFERENT KERNELS

	kernel	Number of Experiments	Acc. (%)	Sens. (%)	Spec. (%)
SD	**Linear**	218,025	**96.51**	**93.98**	**97.77**
	Quadratic	218,025	87.63	69.81	96.53
	Polynomial (3rd order)	218,025	90.24	80.51	95.11
Mean	**Linear**	218,025	**100**	**99.99**	**100**
	Quadratic	218,025	99.34	99.98	99.03
	Polynomial (3rd order)	218,025	99.77	99.31	100

The accuracy, sensitivity, and specificity well conformed to the scatter plots in Fig. 6. The only linear kernel was sufficient, and it performed consistently well in all measurements. The fact that a small kernel yielded relative good results also suggests that MFCC is a viable and practical feature, which has robust discriminating capability.

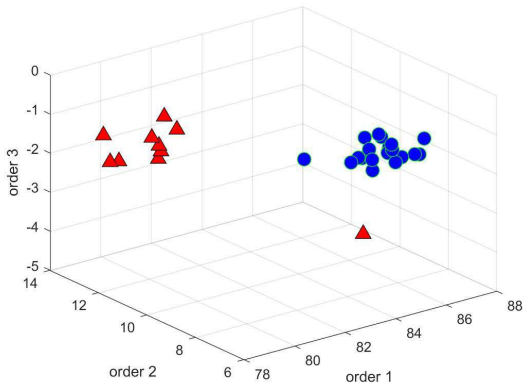

(a) Mean Feature Vectors

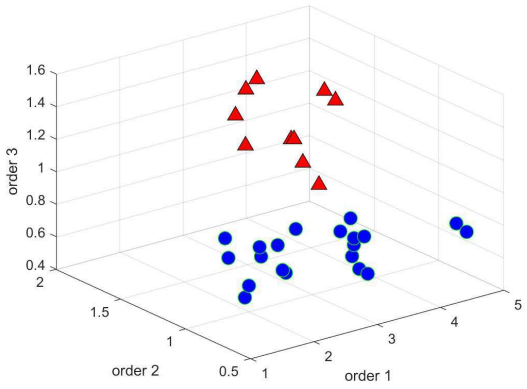

(b) Standard Deviation Feature Vectors

Fig. 6 Comparison of scatter plots between AD (diamond markers) and NC (circle markers) based on Mean (a) and Standard Deviation (b) feature vectors. Axes x, y, and z correspond to 1st, second and third orders MFCC, respectively.

The next experiment was carried out to determine, given a linear kernel, the appropriate cut-off for MFCC orders. The same measures, i.e., accuracy, sensitivity, and specificity were compared, and the results are presented in Table IV. For the standard deviation feature vectors, the SVM required only 5 orders to produce optimal results, whereas, for the mean ones, it required 11–13 orders to fulfill the similar objective.

Similar experiments were also performed but using CNN classifier instead of SVM. Due to a limited number of training sample available, however, the results are not so satisfactory. With the same PET dataset, CNN failed to a classified AD from NC. It is therefore anticipated that, provided a sufficient amount of data, it is worth considering CNN as a viable alternative.

Finally, to determine a minimum bound on the number of MFCC orders, Fig. 7 shows minimum, maximum, averaged, and median accuracies, taken into account different numbers of MFCC orders.

It can be concluded from the figure that to produce a high classification accuracy, one would require at least 3 orders of MFCC. This number may serve as a guideline in designing a practical clinical solution based on the proposed scheme.

TABLE IV
COMPARISON OF SVM CLASSIFICATION WITH DIFFERENT MFCC ORDERS

	MFCC order	Accuracy (%)	Sensitivity (%)	Specificity (%)
SD	1	44.01	29.61	51.21
	2	83.41	68.31	90.96
	3	99.64	98.93	100
	4	99.75	99.24	100
	5	**99.94**	**99.81**	**100**
	6	99.92	99.76	100
	7	98.76	96.30	99.98
	8	99.09	9747	99.90
	9	98.79	97.67	99.35
	10	98.24	96.22	99.25
	11	96.01	91.08	98.47
	12	96.18	92.09	98.23
	13	96.51	93.98	97.77
Mean	1	93.33	90.00	95.00
	2	96.67	90.00	100
	3	97.19	91.56	100
	4	96.77	90.30	100
	5	96.68	90.04	100
	6	99.31	97.94	100
	7	97.19	91.57	100
	8	99.98	99.93	100
	9	99.72	99.15	100
	10	99.84	99.52	100
	11	**100**	**99.99**	**100**
	12	100	99.99	100
	13	100	99.99	100

IV. CONCLUSION

This paper proposed a novel application of Mel-Frequency Cepstral Coefficients (MFCC) as a feature extraction for the early Alzheimer's disease classification from PET scans. The extract features were numerically proved effective and offered high discrimination capability. Although it was first devised for speech applications, the experiments showed that it could be equally well applied to unwrapped 2D PET scans. Thanks to MFCC ability to adjust signal spectra on both frequency and intensity axes, based on localized energy, the underlying signals derived from different sources (or AD and NC classes in our case) can be effectively discriminated, by using only a few MFCC orders. This contribution has been demonstrated in the experiments by applying an SVM as classifiers. The resultant classification yielded overall high accuracy, sensitivity and specificity rate of 96.51%, 93.98%, and 97.77%, respectively. The guideline on how to choose optimal and minimum orders was also given. Despite a limit sample size when building the model, the Leave-p-out cross-validation experiment confirmed that there was no apparent overfitting.

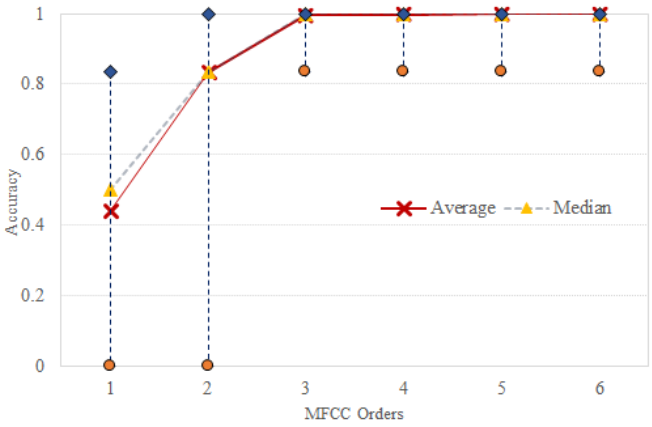

Fig. 7 Minimum, maximum, averaged and median classification accuracies based on a different number of orders included.

ACKNOWLEDGMENT

The authors thank Assoc. Prof. Supatporn Tepmongkol, M.D. for valuable clinical advice. This work was financially supported by the Research Grant of Burapha University through National Research Council of Thailand (Grant no. 116/2557 and 128/2558). PET images employed in this study were provided by King Chulalongkorn Memorial Hospital, Chulalongkorn University, Thailand.

REFERENCES

[1] M. Prince and et al., World Alzheimer Report 2016: Improving healthcare for people living with dementia, Alzheimer's Disease International, 2016.

[2] *What Is Dementia?*, NIA Alzheimer's and related Dementias Education and Referral Center, 2017.

[3] Alzheimer's Association, *2018 Alzheimer's disease facts and figures*, Alzheimer's Association/Alzheimer's & Dementia, vol. 14 (3), pp. 367-429, 2018.

[4] *Alzheimer's Disease Fact Sheet*, NIA Alzheimer's and related Dementias Education and Referral Center**,** 2017.

[5] S. Suksuphew, P. Horkaew, "Hyperplanar Morphological Clustering of a Hippocampus by Using Volumetric Computerized Tomography in Early Alzheimer's Disease." *Brain Sci*., vol. 7, 155. 2017.

[6] A. Khaminkure, J. Panyavaraporn, and P. Horkaew, "Building a Brain Atlas based on Gabor Texture Features," in *Proc. 14th International Joint Conference on Computer Science and Software Engineering*, pp. 1-5, July 2017.

[7] L. Rice, S. Bisdas, "The diagnostic value of FDG and amyloid PET in Alzheimer's disease—A systematic review," *European Journal of Radiology*, vol. 94, pp. 16-24, Sep. 2017.

[8] D. Lu, K. Popuri, G. W. Ding, R. Balachandar and M. F. Beg, "Multiscale deep neural network-based analysis of FDG-PET images for the early diagnosis of Alzheimer's disease," *Medical Image Analysis*, vol. 46, pp. 26-34, Feb. 2018.

[9] W. Wu, J.Venugopalan, and M. D. Wang, "11C-PIB PET image analysis for Alzheimer's diagnosis using weighted voting ensembles," in *Proc. 2017 39th Annual International Conference of the IEEE Engineering in Medicine and Biology Society*, pp. 3914 – 3917, July 2017.

[10] D. Cheng and M. Liu, "Combining convolutional and recurrent neural networks for Alzheimer's disease diagnosis using PET images," in *Proc. 2017 IEEE International Conference on Imaging Systems and Techniques (IST)*, pp. 1-5, Oct. 2017.

[11] Akhila D B, Shobhana S, A. Lenin Fred and S. N Kumar, "Robust Alzheimer's disease classification based on multimodal neuroimaging," in *Proc. 2016 IEEE International Conference on Engineering and Technology (ICETECH)*, pp. 1-5, March 2016.

[12] I. Garali, M. Adel, S. Bourennane and E. Guedj, "Region-based brain selection and classification on pet images for Alzheimer's disease computer-aided diagnosis," in *Proc. 2015 IEEE International Conference on Image Processing (ICIP)*, pp. 1473 - 1477, Sep. 2015.

[13] Fatma El-Zahraa A. El-Gamal, and et. al. "A novel CAD system for local and global early diagnosis of Alzheimer's disease based on PIB-PET scans," in *Proc. 2017 IEEE International Conference on Image Processing (ICIP)*, pp. 3270 – 3274. Sept. 2017

[14] H. Byun and S.-W. Lee, "Applications of Support Vector Machines for Pattern Recognition: A Survey," *LNCS*, 2388, pp. 213-236, 2002.

[15] F. H. Anuwar and A. M. Omar, "Future Solar Irradiance Prediction Using Least Square Support Vector Machine," *International Journal on Advanced Science, Engineering and Information Technology*, 6(4), pp. 520-513, 2016.

[16] N. N. M. Hasri, N. H. Wen, C. W. Howe, M. S. Mohamad, S. Deris and S. Kasim, "Improved Support Vector Machine Using Multiple SVM-RFE for Cancer Classification," *International Journal on Advanced Science, Engineering and Information Technology*, 7(4-2), pp. 1589-1594, 2017.

[17] C. K. On, P.M. Pandiyan, and S.Yaacob, "Mel-frequency cepstral coefficient analysis in speech recognition," in *Proc. International Conference on Computing & Informatics*, pp. 1-5, 2006.

[18] F. S. Al-Anzi, D. Abu Zeina, "The Capacity of Mel Frequency Cepstral Coefficients for Speech Recognition," *International Journal of Computer and Information Engineering*, 11(10), pp. 1162-1166, 2017.